

PIEMAP: Personalized Inverse Eikonal Model from cardiac Electro-Anatomical Maps

Thomas Grandits^{1,4}, Simone Pezzuto², Jolijn M. Lubrecht², Thomas Pock^{1,4},
Gernot Plank^{3,4}, Rolf Krause²

¹ Institute of Computer Graphics and Vision
Graz University of Technology

{thomas.grandits,pock}@icg.tugraz.at

² Center for Computational Medicine in Cardiology,
Institute of Computational Science,
Università della Svizzera italiana,
Lugano, Switzerland

{simone.pezzuto,jolijn.marieke.lubrecht,rolf.krause}@usi.ch

³ Institute of Biophysics

Medical University of Graz

gernot.plank@medunigraz.at

⁴ BioTechMed-Graz, Austria

Abstract. Electroanatomical mapping, a keystone diagnostic tool in cardiac electrophysiology studies, can provide high-density maps of the local electric properties of the tissue. It is therefore tempting to use such data to better individualize current patient-specific models of the heart through a data assimilation procedure and to extract potentially insightful information such as conduction properties. Parameter identification for state-of-the-art cardiac models is however a challenging task.

In this work, we introduce a novel inverse problem for inferring the anisotropic structure of the conductivity tensor, that is fiber orientation and conduction velocity along and across fibers, of an eikonal model for cardiac activation. The proposed method, named PIEMAP, performed robustly with synthetic data and showed promising results with clinical data. These results suggest that PIEMAP could be a useful supplement in future clinical workflows of personalized therapies.

1 Introduction

Patient-specific modeling in cardiac electrophysiology has nowadays reached the status of a clinically feasible tool for assisting the cardiologist during the thera-

This research was supported by the grants F3210-N18 and I2760-B30 from the Austrian Science Fund (FWF) and BioTechMed Graz flagship award "ILearnHeart", as well as ERC Starting grant HOMOVIS, No. 640156. This work was also financially supported by the Theo Rossi di Montelera Foundation, the Metis Foundation Sergio Mantegazza, the Fidinam Foundation, the Horten Foundation and the CSCS—Swiss National Supercomputing Centre production grant s778.

peutic intervention. As models became more mature, and thanks to the increasingly availability of high-resolution data such as high-density electroanatomic maps (EAMs), parameter identification has emerged as a key topic in the field.

A high-density EAM is composed by a large number of contact recordings (1000 points or more), each with local electrogram and spatial information. Activation and conduction velocity maps, for instance, can be derived by combining electric and geometric data. Conductivity parameters in a propagation model may therefore be adapted to reproduce such maps for model personalization.

The reconstruction of conduction velocity maps is generally based on local approaches [4,7]. In these methods, the local front velocity is estimated from an appropriate interpolation of the local activation time (LAT). Anisotropic conductivity can be deduced from front velocity and prior knowledge on fiber structure (rule-based or atlas-based), or by combining multiple activation maps [11].

Although being computationally cheap, these local methods may miss effective mechanisms for global consistency in electric wave propagation models, and may introduce artefacts in conduction velocity due to front collisions or breakthroughs. A different approach, also adopted in this work, relies instead on the (possibly strong) assumption that a calibrated model for the cardiac activation can reproduce the measured activation with sufficient accuracy. The electric conductivity in the model is eventually identified through an optimization procedure aiming at minimizing the mismatch between the model output and the collected data. The model can either be enforced pointwise, yielding for instance PDE-constrained optimization [2], or act as a penalization term [12].

To the best of our knowledge, however, the problem of estimating *simultaneously* distributed fiber architecture and conduction velocities from sparse contact recordings has never been attempted before with either approaches. In this work we aim to bridge this gap by proposing a novel method to extract from a single EAM the full electric conductivity tensor, with the only assumption of symmetric positive-definiteness (s.p.d.) of the tensor field. Local fiber orientation and conduction velocities are then deduced from the eigendecomposition of the conductivity tensor. As forward model, we consider the anisotropic eikonal model, which is a good compromise between physiological accuracy and computational cost [6]. The corresponding inverse model, employing Huber regularization, a smooth total variation approximation, to stabilize the reconstruction and log-Euclidean metric in the parameter space to ensure s.p.d. of the tensor field, is solved by an iterative quadratic approximation strategy combined using a Primal-Dual optimization algorithm. Finally, we extensively test the algorithm with synthetic and clinical data for the activation of the atria, represented as a 2-D manifold, showing promising results for its clinical applicability.

2 Methods

2.1 Forward Problem

The anisotropic eikonal equation describes the activation times u of a wave propagating with direction-dependent velocity. Given a smooth 2-D manifold

$\Omega \subset \mathbb{R}^3$, the equation reads as follows

$$\begin{aligned} \sqrt{\langle D(\mathbf{x}) \nabla_{\mathcal{M}} u(\mathbf{x}), \nabla_{\mathcal{M}} u(\mathbf{x}) \rangle} &= 1 \text{ s.t.: } \forall \mathbf{x} \in \Omega : D_3(\mathbf{x}) \in \mathcal{P}(3) \\ \forall \mathbf{x} \in \Gamma_0 \subset \partial\Omega : u(\mathbf{x}) &= 0, \end{aligned} \quad (1)$$

with Γ_0 representing the domain of fixed activation times, $\mathcal{P}(n)$ being the space of $n \times n$ symmetric positive definite matrices and $\nabla_{\mathcal{M}}$ being the surface gradient. The conductivity tensor $D(\mathbf{x})$ specifies the conduction velocity in the propagation direction, that is $\sqrt{\langle D(\mathbf{x}) \mathbf{k}, \mathbf{k} \rangle}$ is the velocity of the wave at $\mathbf{x} \in \Omega$ in direction \mathbf{k} , \mathbf{k} unit vector.

To solve Eq. (1), we based our algorithm—purely implemented in TensorFlow to allow for automatic gradient computation through back-propagation—on the Fast Iterative Method (FIM) for triangulated surfaces [8]. The only fixed assumed point in PIEMAP $\{\mathbf{x}_0\} = \Gamma_0$ is the chosen earliest activation site, which is assumed to be the earliest of all measured activation points. We use a slightly altered fixed-point iteration $\mathbf{u}^{k+1} = F(\mathbf{u}^k)$ which iteratively updates the activation times. For sake of simplicity, we keep denoting by $u(\mathbf{x})$ the piecewise linear interpolant of the nodal values u_i and by D a piecewise constant tensor field on the triangulated surface. The approximated solution of the equation (1), henceforth denoted by $\text{FIM}_D(\mathbf{x})$ is then the unique fixed-point of the map F . Specifically, the map F updates each of the nodal values as follows:

$$u_i^{k+1} = \begin{cases} 0, & \text{if } \mathbf{x}_i \in \Gamma_0, \\ \underset{T_j \in \omega_i}{\text{smin}}^{\kappa} \underset{\mathbf{y} \in e_{i,j}}{\text{smin}}^{\kappa} \left\{ u(\mathbf{y}) + \sqrt{\langle D_j^{-1}(\mathbf{y} - \mathbf{x}_i), \mathbf{y} - \mathbf{x}_i \rangle} \right\}, & \text{otherwise.} \end{cases} \quad (2)$$

where ω_i is the patch of triangles T_j connected to the vertex \mathbf{x}_i , $e_{i,j}$ is the edge of the triangle T_j opposite to the vertex \mathbf{x}_i , $D_j = D|_{T_j}$ and smin^{κ} being the soft-minimum function, defined as $\text{smin}^{\kappa}(\mathbf{x}) = -\frac{1}{\kappa} \log(\sum_i \exp(-\kappa x_i))$.

Differently from the classic FIM method [8], we concurrently update *all* the nodes, that is the map F is applied in parallel to each node and not just on a small portion of “active” nodes. We also replaced the min-function of the original FIM-algorithm by the soft-minimum smin^{κ} to ensure a limited degree of smoothness of the function and avoid discontinuities in the gradient computation.

2.2 PIEMAP and inverse problem

PIEMAP implements an inverse problem in which the optimal conductivity tensor field D for Eq. (1) is selected such that the mismatch between recorded activation times $\hat{u}(\mathbf{x})$ and the simulated activation times $\text{FIM}_D(\mathbf{x})$ on the measurement domain $\Gamma \subset \Omega$ is minimized in the least-squares sense.

In principle, after accounting for symmetry, $D(x)$ has 6 component to be identified for every $x \in \Omega$. Since the dynamic of the wave propagation is bound to the 2-D manifold, however, the component normal to the surface does not influence the solution. We therefore define $D(\mathbf{x})$ as follows:

$$D(\mathbf{x}) = P(\mathbf{x}) \begin{pmatrix} \tilde{D}(\mathbf{x}) & \mathbf{0} \\ \mathbf{0}^{\top} & 1 \end{pmatrix} P(\mathbf{x})^{\top}, \quad (3)$$

where $\tilde{D}(\mathbf{x}) \in \mathcal{P}(2)$ and $P(x)$ is a rotation from the canonical base in \mathbb{R}^3 to a local base $\{\mathbf{v}_1(\mathbf{x}), \mathbf{v}_2(\mathbf{x}), \mathbf{n}(\mathbf{x})\}$. The local base at $\mathbf{x} \in \Omega$ is such that $\mathbf{n}(\mathbf{x})$ is the normal vector to the surface and $\mathbf{v}_1(\mathbf{x}), \mathbf{v}_2(\mathbf{x})$ span the tangent space. In such way, the dimension of the parameter space is reduced from 6 to only 3. Any basis $\mathbf{v}_1(\mathbf{x})$ in the tangent space is valid, but we compute a smooth basis by minimizing the variation across the manifold:

$$\min_{\mathbf{v}_1} \int_{\Omega} \|\nabla \mathbf{v}_1(\mathbf{x})\|_2^2 d\mathbf{x} \quad \text{s.t.: } \forall \mathbf{x} \in \Omega : \|\mathbf{v}_1(\mathbf{x})\| = 1,$$

to ensure a meaningful result through the later introduced regularization term. The computed local bases, used in all experiments throughout this paper, are shown in Fig. 1. Finally, we consider the Log-Euclidean metric [1] for ensuring

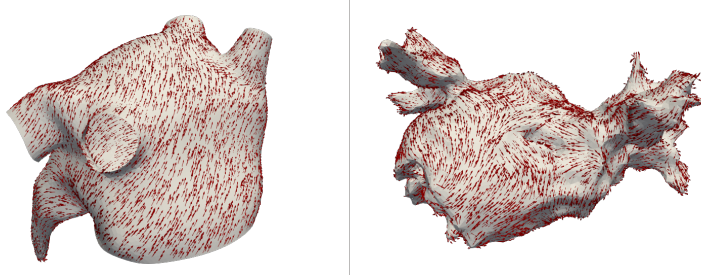


Fig. 1. Generated local bases on the atria manifold models.

a s.p.d. tensor field: given $\mathbf{d}(\mathbf{x}) \in \mathbb{R}^3$, $\mathbf{x} \in \Omega$, we set \tilde{D} as follows:

$$\tilde{D}(\mathbf{x}) := \exp \begin{pmatrix} d_1(\mathbf{x}) & d_2(\mathbf{x}) \\ d_2(\mathbf{x}) & d_3(\mathbf{x}) \end{pmatrix}, \quad (4)$$

where the matrix exponential is computed from the eigendecomposition. In particular, the admissible set \mathbb{R}^3 is mapped through (3) and (4) to $\mathcal{P}(3)$.

The inverse problem, therefore, consists in finding the vector field $\mathbf{d} \in \mathbb{R}^3$, which minimizes the following objective function:

$$\min_{\mathbf{d}} \underbrace{\frac{1}{2} \int_{\Gamma} (\text{FIM}_{D(\mathbf{d})}(\mathbf{x}) - \hat{u}(\mathbf{x}))^2 d\mathbf{x}}_{U(\mathbf{d})} + \lambda \underbrace{\int_{\Omega} H_{\epsilon}(\nabla_{\mathcal{M}} \mathbf{d}) d\mathbf{x}}_{\text{TV}_{\epsilon, \lambda}(\mathbf{d})}, \quad (5)$$

where $\text{TV}_{\epsilon, \lambda}(\mathbf{d})$ is a smooth total variation (TV) regularization term which alleviates the ill-posedness of the problem. Specifically, H_{ϵ} is the Huber function:

$$H_{\epsilon}(\mathbf{x}) = \begin{cases} \frac{1}{2\epsilon} |\mathbf{x}|^2, & \text{if } |\mathbf{x}| \leq \epsilon, \\ |\mathbf{x}| - \frac{1}{2}\epsilon, & \text{else} \end{cases} \quad (6)$$

We set $\epsilon = 0.05$ for our experiments, while the optimal choice of regularization parameter λ is obtained by using a cross-validation approach.

2.3 Forward-Backward Splitting and Numerical Solution

The computational complexity of solving Eq. (5) is dominated by the time for computing FIM_D and $\nabla_{\mathbf{d}}\text{FIM}_D$. The implementation of FIM_D in TensorFlow allows for an efficient computation of $\nabla_{\mathbf{d}}\text{FIM}_D$ via backpropagation on a graphical processing unit (GPU). While the minimization of the residual $U(\mathbf{d})$ is usually achieved very quickly, at least when \hat{u} is a (possibly corrupted) solution of Eq. (1), the TV term tends to increase the number of needed iterations for convergence. In order to increase the convergence rate, we apply the principle of the Fast Iterative Shrinking and Thresholding Algorithm (FISTA) [3], quadratically bounding the non-linear, non-convex function U around the current point \mathbf{d}_k :

$$U(\mathbf{d}) \leq U(\mathbf{d}_k) + \langle \nabla_{\mathbf{d}}U(\mathbf{d}_k), (\mathbf{d} - \mathbf{d}_k) \rangle + \frac{L}{2} \|\mathbf{d} - \mathbf{d}_k\|_2^2 =: G(\mathbf{d}). \quad (7)$$

The bounding function $G(\mathbf{d})$ is convex, hence has a unique minimum $\bar{\mathbf{d}} = \mathbf{d}_k - L^{-1}\nabla_{\mathbf{d}}U(\mathbf{d}_k)$. As $\text{TV}_{\varepsilon,\lambda}(\mathbf{d})$ is also convex, we obtain the following convex minimization problem:

$$\min_{\mathbf{d}} \frac{L}{2} \|\mathbf{d} - \bar{\mathbf{d}}\|_2^2 + \text{TV}_{\varepsilon,\lambda}(\mathbf{d}).$$

Iteratively solving this class of problems along with an acceleration term is usually referred to as FISTA. We recast the problem into a convex-concave saddle-point problem:

$$\min_{\mathbf{d}} \max_{\mathbf{p}} \frac{L}{2} \|\mathbf{d} - \bar{\mathbf{d}}\|_2^2 + \langle \nabla_{\mathcal{M}}\mathbf{d}, \mathbf{p} \rangle - \text{TV}_{\varepsilon,\lambda}^*(\mathbf{p}) \quad (8)$$

which can be solved using the Primal-Dual algorithm [5] given by:

$$\begin{cases} \mathbf{d}^{i+1} = \text{prox}_{\tau G}(\mathbf{d}^i - \tau \nabla_{\mathcal{M}}^* \mathbf{d}^i) \\ \mathbf{d}_{\Theta} = \mathbf{d}^{i+1} + \theta (\mathbf{d}^{i+1} - \mathbf{d}^i) \\ \mathbf{p}^{i+1} = \text{prox}_{\sigma \text{TV}_{\varepsilon,\lambda}^*}(\mathbf{p}^i + \sigma \nabla_{\mathcal{M}} \mathbf{d}_{\Theta}) \end{cases} \quad (9)$$

with

$$\begin{aligned} \hat{\mathbf{d}} &= \text{prox}_{\tau U}(\tilde{\mathbf{d}}) = (\tilde{\mathbf{d}} + \tau L \tilde{\mathbf{d}}) / (\tau L + 1) \\ \hat{\mathbf{p}} &= \text{prox}_{\sigma \text{TV}_{\varepsilon,\lambda}^*}(\mathbf{p}) \Leftrightarrow \hat{\mathbf{p}}_j = \begin{cases} \frac{\bar{\mathbf{p}}_j}{|\bar{\mathbf{p}}_j|/\lambda} & \text{if } |\bar{\mathbf{p}}_j| > 1 \\ \bar{\mathbf{p}}_j & \text{else} \end{cases} \end{aligned}$$

for $\bar{\mathbf{p}}_j = \frac{\mathbf{p}_j}{\sigma\varepsilon/\lambda+1}$, $\theta = 1$ and $\tau\sigma\|\nabla_{\mathcal{M}}\|_2^2 \leq 1$. The parameter L in Eq. (7), usually challenging to evaluate, is computed through a Lipschitz backtracking algorithm [3].

3 Experiments

For the evaluation of PIEMAP, we first assessed its effectiveness on reconstructing known conduction velocity and fibers on a realistic human left atrium (LA) model, also in the presence of white noise and heterogeneity. The LA model was generated from MRI data of a patient, with the fibers semi-automatically assigned as described previously [9]. Fiber and transverse velocity were set to $0.6 \frac{\text{m}}{\text{s}}$ and $0.4 \frac{\text{m}}{\text{s}}$ respectively for the entire LA, except for the low conducting region, where we used $0.2 \frac{\text{m}}{\text{s}}$ for both fiber and transverse velocity. We tested PIEMAP both in the case of fully anisotropic and in the case of isotropic conduction. In the latter case, in particular, we compared PIEMAP to existing methods for the evaluation of conduction velocity, namely a local method [4] and EikonalNet [12], a Physics Informed Neural Network (PINN) method. In a second set of experiments, we eventually applied PIEMAP to clinically acquired data, in the form of high-density EAM.

All experiments were run on a desktop machine with an Intel Core i7-5820K CPU with 6 cores of each 3.30GHz, 32GB of working memory and a NVidia RTX 2080 GPU. All examples were optimized for 2000 iterations, with each iteration taking about 1.8 seconds, totalling into a run-time of approximately 1 hour for one optimization.

3.1 Numerical assessment

All the experiments were performed on a human, cardiac magnetic resonance (CMR)-derived left atrium model, with semi-automatically placed fiber directions based on histological studies. The ground-truth (GT) solution was computed with a single earliest activation site using Eq. (1), and with a low-conducting area being close to the left atrial appendage. Different levels of independent and identically distributed (i.i.d.) Gaussian noise with standard deviation σ_N were tested. The measurement domain was a set of 884 points uniformly distributed across the atrium. The reconstruction root-mean-square error (RMSE) with respect to GT was evaluated in terms of conduction velocity (m/s), propagation direction and, only for PIEMAP, fiber-angle error. To evaluate the results, we compute the front direction and fiber direction unit vectors, denoted as \mathbf{e} and \mathbf{f} respectively. The front and fiber angle-errors are then defined as $\alpha_{\mathbf{e}} = \arccos \langle \mathbf{e}, \mathbf{e}_{\text{GT}} \rangle \in [0, 180^\circ)$ and $\alpha_{\mathbf{f}} = \arccos |\langle \mathbf{f}, \mathbf{f}_{\text{GT}} \rangle| \in [0, 90^\circ)$. The velocity errors in propagation direction are then $v \cos(\alpha_{\mathbf{x}}) - v_{\text{GT}}$ for computed velocity v and exact velocity v_{GT} , both in the front and fiber direction.

Results are reported in Tab. 1. All methods correctly captured the low conduction region. PIEMAP compared favourably to the local method at all noise levels in terms of absolute conduction velocity. EikonalNet shows a slightly more accurate front angle error, which is counteracted by the considerably high front velocity error, both compared to our and the local method.

Overall, PIEMAP had the benefit over EikonalNet that the GT was generated with the anisotropic eikonal model, and thus it is in theory possible to reproduce the data exactly with a zero noise level. In the local method no model as-

Table 1. Comparison of the front-velocity/front-angle error of PIEMAP with the local approach [4] and EikonalNet [12], assuming different noise levels for the in-silico models. Errors in $\frac{m}{s}$ /degree. In the last column, we compare the fiber velocity error and fiber angle error.

		Error in Propagation Direction			Fiber Error
		PIEMAP	Local Method	EikonalNet	PIEMAP
σ_N/PSNR	0ms/ ∞ dB	0.20 /10.58	0.20 /22.95	0.53/ 9.20	0.25/38.34
	0.1ms/64.1 dB	0.19 /10.61	0.20/23.17	0.40/ 9.10	0.25/38.46
	1ms/43.9 dB	0.20 / 11.03	0.21/23.57	0.49/14.60	0.25/38.59
	5ms/29.9 dB	0.25 / 19.94	0.29/30.20	1.24/49.40	0.26/40.14

sumption is made. Interestingly, the error in front direction for the local method could be linked to the fact that, in the presence of anisotropic conduction, propagation direction and $\nabla_{\mathcal{M}}u$ differ. For instance, a circular propagation from the source x_0 satisfies Eq. (1) with $u(x) = \sqrt{\langle D^{-1}(x - x_0), (x - x_0) \rangle}$, thus $\nabla_{\mathcal{M}}u$ differs from $x - x_0$, which is the propagation direction. In the local method, $\nabla_{\mathcal{M}}u$ is used to establish such direction. In EikonalNet, results were less robust to noise. A plausible explanation is that training Neural Networks does not always yield the same results, as multiple local minima might be present. Therefore, error can be slightly lower or higher depending on the initial conditions. In terms of computational time, PIEMAP was comparable to EikonalNet, but significantly slower than the local method.

Regarding the reconstruction of fiber directions (see Fig. 2), we observed a very good performance for the fiber and cross-fiber velocity, and a reasonable reconstruction for the direction. In particular, reconstruction in fiber direction was poor around the boundaries (mitral ring and pulmonary veins, where fibers run parallel to the opening) and in the scarred region, which attribute the most to the fiber angle error in Tab. 1. The distribution of fiber angle errors is a slightly left-skewed uniform distribution (not shown), indicating that the chosen smooth basis along with a simple TV prior can provide resonable results with respect to the activation timings. Still, it may not be sufficient to account for the partly complicated fiber orientation, especially in areas of high-curvature of the mesh or sudden changes of fiber orientation on the endocardium as an effect of the volumetric structure of the atria, such as is the case for the mitral valve. Physiological priors will need to be considered in the future for this purpose.

3.2 Application to real clinical data

In a patient candidate to ablation therapy, a high-density activation map along with a 3D patient-specific atrial model was acquired with an EAM system (Catheter: Pentaray® System: CARTO® 3 System, Biosense Webster). The recordings encompassed roughly 850 “beats” of 2.5 sec including both the electrode position in 3D space and the unipolar electrogram (1 kHz). Recordings that were deemed to be untrustworthy due to 1) insufficient contact, 2) sliding

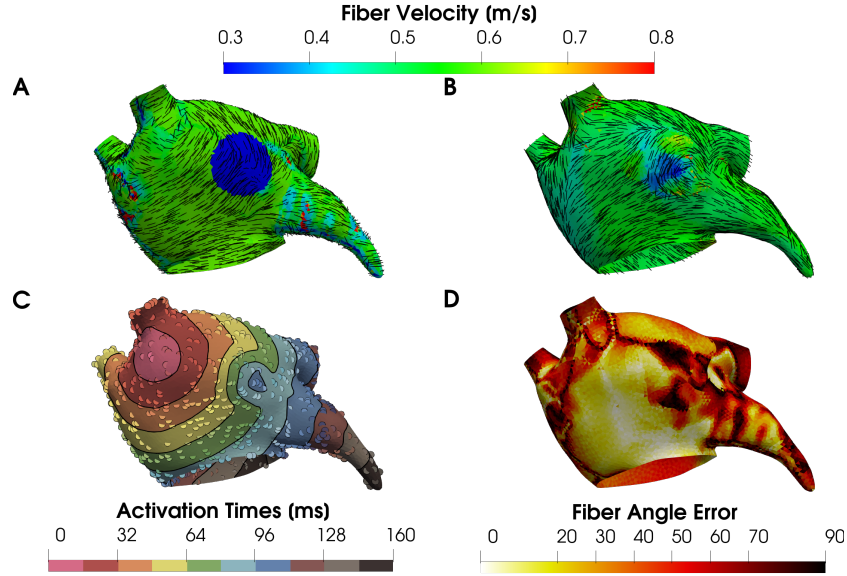


Fig. 2. Results of our method on the noise-less LA-model with known ground-truth fiber orientation and velocity (A). The scarred region is correctly activated at a later time by a combination of reducing fiber-velocity, as well as aligning fibers along the contour lines (B/C). The activation map can faithfully capture the observed measurement points $u(\mathbf{x} \in \Gamma)$, marked as colored dots (C) and matches the GT-model's activation closely (not shown). Fiber alignment of our model (B) shows mostly errors around the mitral valves, the scarred region and pulmonary veins (D), as well as regions of high curvature. Best viewed online.

of the electrode in 3D space >1 cm, 3) correspondence to a inconsistent surface P-wave, 4) minimal unipolar amplitude, were excluded automatically from the study. To avoid degenerated triangles with acute angles, sometimes created by the EAM recordings, we used PyMesh⁵ to postprocess the mesh. A further manual pre-processing of the signals was eventually performed for a correct detection of the local activation time (steepest negative deflection in the unipolar signal) in the last beat and compared to local bipolar signals for confirmation. Distribution of points was uneven across the LA, as many points were located around the pulmonary veins (PVs).

Of the remaining valid 565 beats, randomly chosen 80% (452 points) were used to optimize Eq. (5), while the remaining 20% were used as a cross-validation set to find the optimal regularization parameter λ . Fig. 3 shows the fiber velocity, orientation and activation map after the optimization. The cross-validation error over several values of λ is shown in Fig. 4, which lead us to the used value of λ . The best cross-validation error lead to a relatively smooth fiber velocity field, with velocities ranging up to $1.5 \frac{m}{s}$ in the initiation region, probably a con-

⁵ <https://github.com/PyMesh/PyMesh>

sequence of choosing only one mesh node as an initiation site when in reality the initiation site is larger or composed of multiple sites. A speed-up of propagation near the atrial wall can often be witnessed and is compensated in our model by an overall higher fiber-velocity.

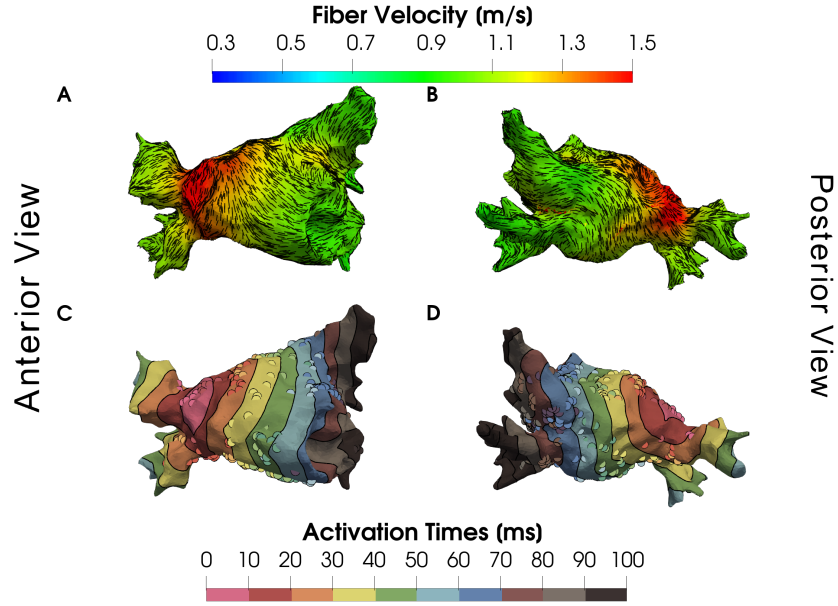


Fig. 3. Anterior (A/C) and posterior view (B/D) of PIEMAP’s results on a patient’s left atria. The panels A and B show the found fiber direction and fiber velocity, while the panels C and D show the activation map along with the actual measured points on top, similar to Fig. 2.

4 Discussion & Conclusion

In this paper, we proposed PIEMAP, a global method to reconstruct the conductivity tensor (fiber direction, fiber- and cross-fiber velocity) of an anisotropic eikonal model from sparse measurement of the activation times. We compared our method to existing approaches for determining the conduction velocity map from the same data (a local method and a PINN method) and we demonstrated its effectiveness in a real application.

Our method showed promising results on atrial electrical data, acquired using an EAM system, but may be used with any electrical measurements, mapped to a manifold. In Sec. 3.1, we demonstrated the possibility to infer low conducting regions, as sometimes witnessed for scarred regions, but future studies could apply the algorithm to analyze different pathologies, such as fibrosis.

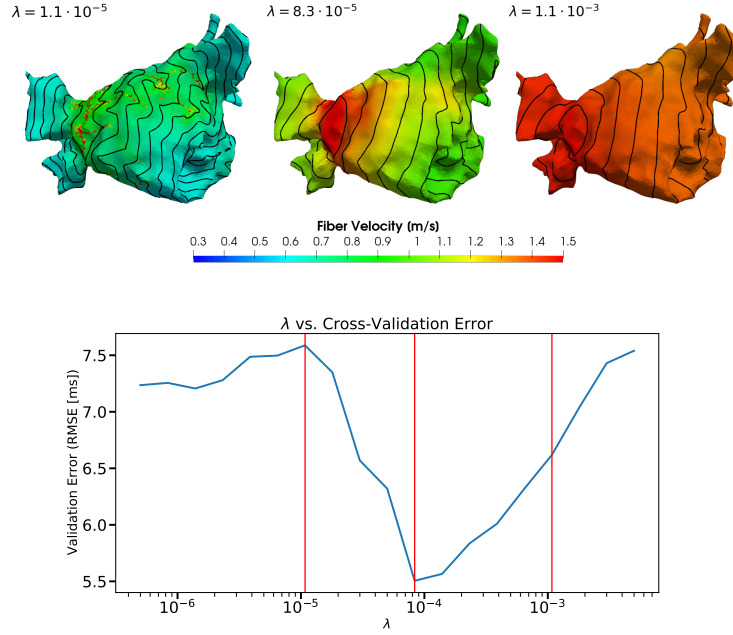


Fig. 4. Influence on the final cross-validation error when varying over λ for the optimization on the EAM recordings. The black contours are the isochrones of the modelled activation. Shown are the results of three different λ values: The left result is the least regularized with $\lambda = 1.1 \cdot 10^{-5}$, while the result on the right side is heavily regularized with $\lambda = 1.1 \cdot 10^{-3}$. A compromise is the figure in the middle with $\lambda = 8.3 \cdot 10^{-5}$, but finding the physiologically most plausible value for λ is a non-trivial task since we do not know the true distribution of velocities and activations in the atria.

With special care for registration, PIEMAP could also be combined with high-resolution 3D imaging, such as CT or MRI, to improve anatomical accuracy. An interesting question is whether PIEMAP could also be applied to ventricular activation. A major difference between ventricular and atrial activation is transmural propagation in the former, which is not accessible by contact mapping. Moreover, endocardial activation in the ventricles of healthy subjects, due to the Purkinje network, is extremely complex and may overshadow myocardial propagation. Under specific pathological conditions, such as ventricular tachycardia or bundle branch block, myocardial activation becomes relevant and heterogeneity in conduction of potential interest, justifying the applicability of PIEMAP. While it is true that no transmural data would be available, it is also known that fibers in ventricles follow a peculiar pattern in the transmural direction with low inter-patient variability [13]. Such *prior knowledge* may be used in the inverse procedure by appropriately changing the regularization term. In a recent work [10], we actually applied an inverse method similar to PIEMAP in the ventricles by using epicardial data, obtaining convincing results also in the transmural direction.

In light of the presented results, we believe that PIEMAP can assist future medical interventions by estimating cardiac conduction properties more robustly and help in identifying ablation sites, as well as in better understanding atrial and ventricular conduction pathways.

References

1. Arsigny, V., Fillard, P., Pennec, X., Ayache, N.: Geometric means in a novel vector space structure on symmetric positive-definite matrices. *SIAM J Matrix Anal Appl* **29**(1), 328–347 (2007). <https://doi.org/10.1137/050637996>
2. Barone, A., Gizzi, A., Fenton, F., Filippi, S., Veneziani, A.: Experimental validation of a variational data assimilation procedure for estimating space-dependent cardiac conductivities. *Comput Method Appl M* **358**, 112615 (2020). <https://doi.org/10.1016/j.cma.2019.112615>
3. Beck, A., Teboulle, M.: A Fast Iterative Shrinkage-Thresholding Algorithm for Linear Inverse Problems. *SIAM J Imaging Sci* **2**(1), 183–202 (2009). <https://doi.org/10.1137/080716542>
4. Cantwell, C., Roney, C., Ng, F., Siggers, J., Sherwin, S., Peters, N.: Techniques for automated local activation time annotation and conduction velocity estimation in cardiac mapping. *Comput Biol Med* **65**, 229–242 (2015). <https://doi.org/10.1016/j.compbio.2015.04.027>
5. Chambolle, A., Pock, T.: A First-Order Primal-Dual Algorithm for Convex Problems with Applications to Imaging. *J Math Imaging Vis* **40**(1), 120–145 (2011). <https://doi.org/10.1007/s10851-010-0251-1>
6. Colli Franzone, P., Guerri, L.: Spreading of excitation in 3-d models of the anisotropic cardiac tissue. I. validation of the eikonal model. *Math Biosci* **113**(2), 145–209 (1993). [https://doi.org/10.1016/0025-5564\(93\)90001-Q](https://doi.org/10.1016/0025-5564(93)90001-Q)
7. Coveney, S., Corrado, C., Roney, C.H., O’Hare, D., Williams, S.E., O’Neill, M.D., Niederer, S.A., Clayton, R.H., Oakley, J.E., Wilkinson, R.D.: Gaussian process manifold interpolation for probabilistic atrial activation maps and uncertain conduction velocity. *Philos T R Soc A* **378**(2173), 20190345 (2020). <https://doi.org/10.1098/rsta.2019.0345>
8. Fu, Z., Jeong, W., Pan, Y., Kirby, R., Whitaker, R.: A Fast Iterative Method for Solving the Eikonal Equation on Triangulated Surfaces. *SIAM J on Sci Comp* **33**(5), 2468–2488 (2011). <https://doi.org/10.1137/100788951>
9. Gharaviri, A., Bidar, E., Potse, M., Zeemering, S., Verheule, S., Pezzuto, S., Krause, R., Maessen, J.G., Auricchio, A., Schotten, U.: Epicardial fibrosis explains increased endo–epicardial dissociation and epicardial breakthroughs in human atrial fibrillation. *Front Phys* **11**, 68 (2020). <https://doi.org/10.3389/fphys.2020.00068>
10. Grandits, T., Gillette, K., Neic, A., Bayer, J., Vigmond, E., Pock, T., Plank, G.: An inverse Eikonal method for identifying ventricular activation sequences from epicardial activation maps. *Journal of Computational Physics* **419**, 109700 (Oct 2020). <https://doi.org/10.1016/j.jcp.2020.109700>, <http://www.sciencedirect.com/science/article/pii/S0021999120304745>
11. Roney, C.H., Whitaker, J., Sim, I., O’Neill, L., Mukherjee, R.K., Razeghi, O., Vigmond, E.J., Wright, M., O’Neill, M.D., Williams, S.E., Niederer, S.A.: A technique for measuring anisotropy in atrial conduction to estimate conduction velocity and atrial fibre direction. *Comput Biol Med* **104**, 278–290 (2019). <https://doi.org/10.1016/j.compbio.2018.10.019>

12. Sahli Costabal, F., Yang, Y., Perdikaris, P., Hurtado, D.E., Kuhl, E.: Physics-Informed Neural Networks for Cardiac Activation Mapping. *Front Phys* **8**, 42 (2020). <https://doi.org/10.3389/fphy.2020.00042>
13. Streeter, D.D., Spotnitz, H.M., Patel, D.P., Ross, J., Sonnenblick, E.H.: Fiber Orientation in the Canine Left Ventricle during Diastole and Systole. *Circ Res* **24**(3), 339–347 (1969). <https://doi.org/10.1161/01.RES.24.3.339>